NANO LETTERS

Letter

pubs.acs.org/NanoLett

Janus Solid–Liquid Interface Enabling Ultrahigh Charging and Discharging Rate for Advanced Lithium-Ion Batteries

Jiaxin Zheng,[†] Yuyang Hou,[#,‡] Yandong Duan,[†] Xiaohe Song,[†] Yi Wei,[†] Tongchao Liu,[†] Jiangtao Hu,[†] Hua Guo,[†] Zengqing Zhuo,[†] Lili Liu,[‡] Zheng Chang,[‡] Xiaowei Wang,[‡] Danylo Zherebetskyy,[§] Yanyan Fang,[∥] Yuan Lin,[∥] Kang Xu,[⊥] Lin-Wang Wang,[§] Yuping Wu,[*,#,‡] and Feng Pan[*,†]

[†]School of Advanced Materials, Peking University, Shenzhen Graduate School, Shenzhen 518055, People's Republic of China

[#]College of Energy, Nanjing Tech University, Nanjing 211816, Jiangsu Province, People's Republic of China

[‡]New Energy and Materials Laboratory (NEML), Department of Chemistry & Shanghai Key Laboratory of Molecular Catalysis and Innovative Materials, Fudan University, Shanghai 200433, People's Republic of China

[§]Materials Science Division, Lawrence Berkeley National Laboratory, Berkely, California 94720, United States

[∥]Beijing National Laboratory for Molecular Sciences, Key Laboratory of Photochemistry, Institute of Chemistry, Chinese Academy of Sciences, Beijing 100190, People's Republic of China

[⊥]Electrochemistry Branch, U.S. Army Research Laboratory, Adelphi, Maryland 20783, United States

Supporting Information

ABSTRACT: $LiFePO_4$ has long been held as one of the most promising battery cathode for its high energy storage capacity. Meanwhile, although extensive studies have been conducted on the interfacial chemistries in Li-ion batteries,[1−3] little is known on the atomic level about the solid–liquid interface of $LiFePO_4$/electrolyte. Here, we report battery cathode consisted with nanosized $LiFePO_4$ particles in aqueous electrolyte with an high charging and discharging rate of 600 C (3600/600 = 6 s charge time, 1 C = 170 mAh g^{-1}) reaching 72 mAh g^{-1} energy storage (42% of the theoretical capacity). By contrast, the accessible capacity sharply decreases to 20 mAh g^{-1} at 200 C in organic electrolyte. After a comprehensive electrochemistry tests and ab initio calculations of the $LiFePO_4$–H_2O and $LiFePO_4$–EC (ethylene carbonate) systems, we identified the transient formation of a Janus hydrated interface in the $LiFePO_4$–H_2O system, where the truncated symmetry of solid $LiFePO_4$ surface is compensated by the chemisorbed H_2O molecules, forming a *half-solid* ($LiFePO_4$) and *half-liquid* (H_2O) amphiphilic coordination environment that eases the Li desolvation process near the surface, which makes a fast Li-ion transport across the solid/liquid interfaces possible.

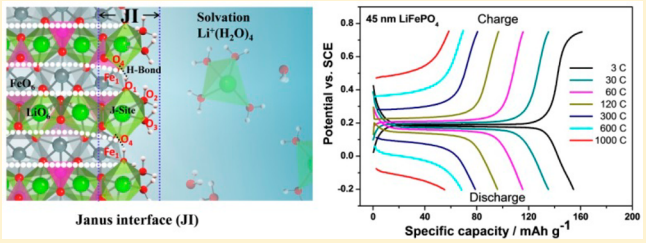

KEYWORDS: *$LiFePO_4$, rate performance, aqueous electrolyte, organic electrolyte, solid–liquid interface, ab initio calculations*

Charging/discharging rate (CDR) is a key battery parameter that dictates how fast energy can be harnessed or released and is critical for applications such as vehicle-electrification and renewable energy grids.[4,5] Although supercapacitors and redox-flow batteries exhibit certain potentials for these applications,[5−7] their capacities are often limited or costs are too high.[8] On the other hand, the high energy and power densities and excellent cycling stability of lithium-ion batteries (LIBs) have made them the most promising candidate. As a safer LIB cathode chemistry, $LiFePO_4$ has been intensively studied in the past decade,[9] whose CDR was found to be surprisingly decoupled from its low intrinsic ionic and electronic conductivities. Previous work has identified that, with nanosized particles, the limiting step is no longer the Li^+-intercalation rate within the particles but rather the transports of Li^+ and electrons to or from them.[10−12] As a commonly used and highly effective practice, carbon coating has successfully addressed the electronic contact among electrode active ingredients,[13] whereas recent experiment and theory suggested that Li^+-transport across the cathode/electrolyte interface might play the dictating role for the $LiFePO_4$ rate performance.[14−17] Gaberscek and co-workers suggested that the "ionic coating" around $LiFePO_4$ might matter more than electronic coating due to the much clumsier ionic movements,[14] and they believe that, at sufficiently small particle sizes, the rate-limiting step should be the interfacial reaction rather than transport within the bulk.

On the other hand, electrolytes also exercise a critical control on the rate performance,[18,19] determining not only Li^+-diffusion within the bulk electrolyte, but also the transport process at solid/electrolyte interface. In recent years aqueous lithium battery has been intensively explored as an alternative to its nonaqueous counterparts, mainly because of the intrinsic safe

Received: June 16, 2015
Revised: August 20, 2015
Published: August 25, 2015

DOI: 10.1021/acs.nanolett.5b02379
Nano Lett. 2015, 15, 6102–6109

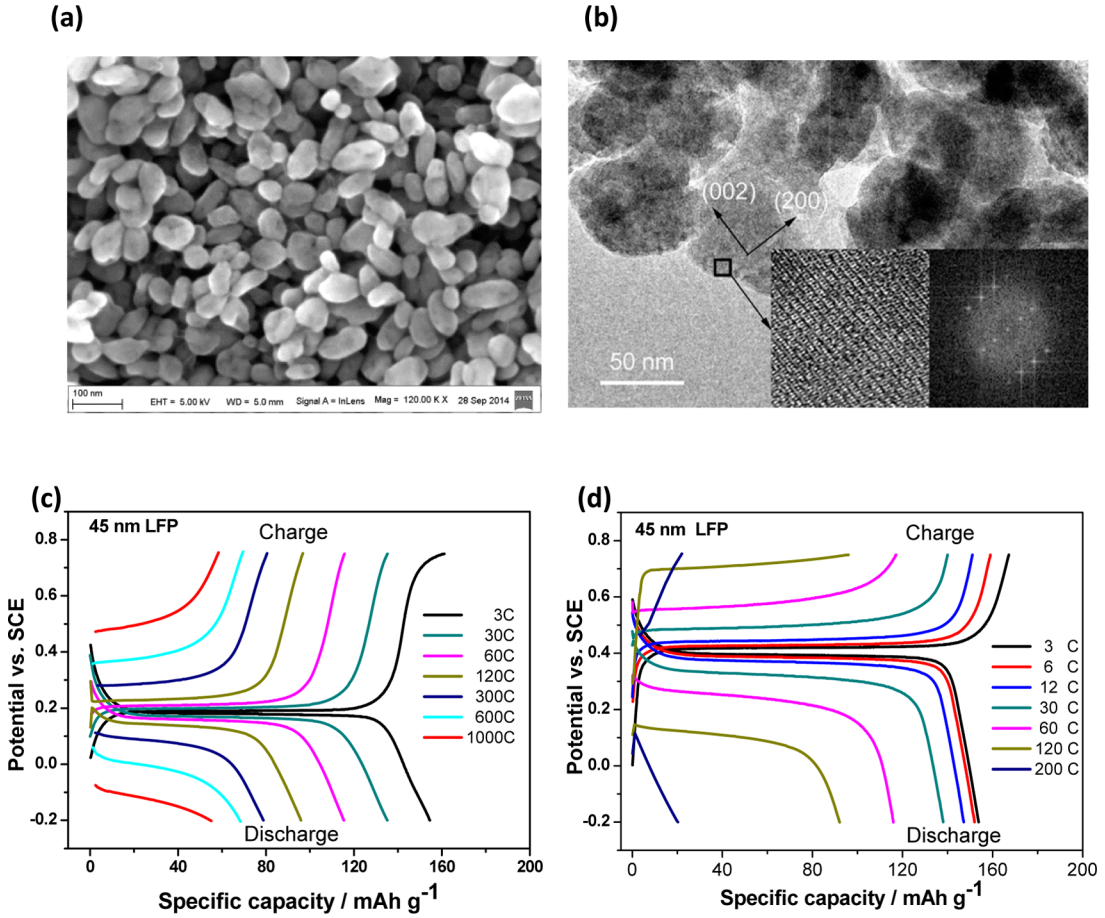

Figure 1. Morphology of the prepared 45 nm $LiFePO_4$ (LFP) nanoparticles and its electrochemical properties. (a) Scan electron micrograph (SEM) of the morphology. (b) Transmission electron micrograph (TEM): large percentage of the surface is (010) faced. (c) and (d) Charge and discharge curves at different current density (1 C = 170 mA g^{-1}) between −0.2 and 0.75 V (vs SCE) in 0.5 M Li_2SO_4 aqueous electrolyte (c) and in an organic electrolyte (1 M $LiClO_4$ electrolyte in a mixture of ethylene carbonate and dimethyl carbonate) (d).

nature brought by the water-based electrolytes.[20−25] However, many fundamental questions regarding how LIB chemistries behave in aqueous and nonaqueous media remains unanswered[16] (Table S2 in Supporting Information), which includes: how differently do organic and aqueous electrolyte interact with electrode surfaces on atomic level, which factor governs the kinetics of Li^+-intercalation/deintercalation processes at the interfaces dissecting solid electrodes from electrolytes, and what would a "perfect" interface be in order for Li^+-transport to occur at ultrahigh rate with minimum resistance?

Here, we report our efforts in addressing these questions by comparing CDRs of $LiFePO_4$ in both aqueous and nonaqueous electrolytes. With cathode consisting of nanosized $LiFePO_4$ in 0.5 M Li_2SO_4 aqueous solution, a rate of 600 C (1 C = 170 mAh g^{-1}) could be achieved for both charging and discharging while still retaining a capacity of 72.0 mAh g^{-1} (42% of the theoretical capacity). By contrast, the accessible capacity sharply decreases to 20 mAh g^{-1} at 200 C in organic electrolyte. We also found that this high rate capability comes with minimum interfacial resistance and excellent cycling stability in aqueous electrolyte, that is, after 400 cycles at 10 C, the loss of capacity is only 5% (less than 15% after 1000 cycles). Combination of these merits makes aqueous LIB using such nanosized $LiFePO_4$ a promising candidate for applications requiring high capacity and high CDR, and with additional benefits such as nonflammability, low cost, and small environmental footprint. All imparted from the aqueous electrolytes, render particular suitability for large-scale energy storage systems (>10^6 Wh), where concerns over the prohibitive high cost of production, operation and maintenance, potential safety hazard, and environmental disaster far outweigh any advantages in energy densities.

Results and Discussion. Different crystallite sizes of $LiFePO_4$ (45 and 101 nm) were prepared by reflux route in ethylene glycol solution under atmospheric pressure. $LiFePO_4$ samples were mixed with 20 wt % of glucose and then carbonized at 650 °C for 6 h in Ar atmosphere. The obtained $LiFePO_4$/C composites were single $LiFePO_4$ phase as determined by X-ray diffraction (XRD) (Figure S1c in Supporting Information). The SEM images of $LiFePO_4$/C are shown in Figure 1a and Figure S1a in Supporting Information. The samples consist of monodispersed nanocrystalline particles with platelet shape, and the high-resolution transmission electron microscopy (HRTEM) images (Figure 1b and Figure S1b in Supporting Information) reveal well-crystallized nanoparticles of 45 and 101 nm. The patterns of fast Fourier transform of HRTEM displayed in the inset of Figure 1b and Figure S1b in Supporting Information indicate that the 45 nm $LiFePO_4$ crystal has a major exposure of (010) facets, whereas the 101 nm $LiFePO_4$ grows transversely along the (010) direction.

DOI: 10.1021/acs.nanolett.5b02379
Nano Lett. 2015, 15, 6102−6109

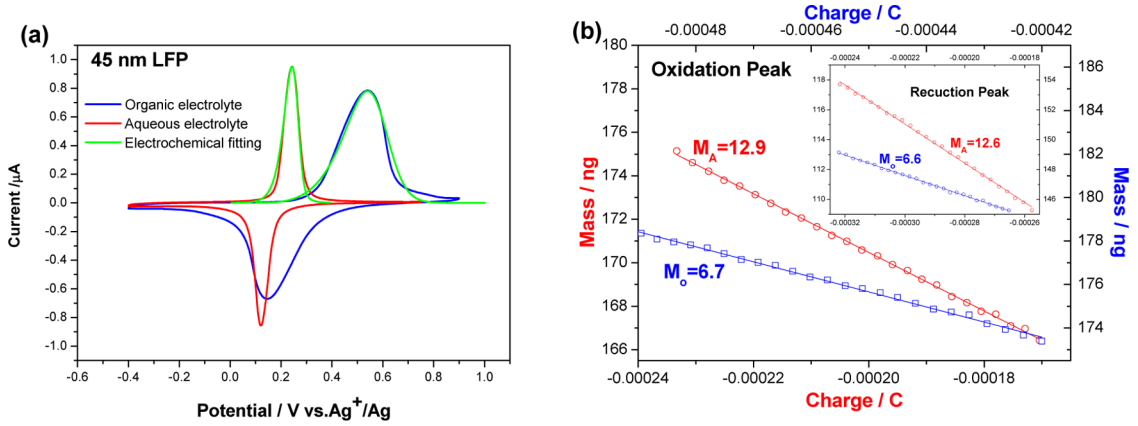

Figure 2. Kinetic properties of the electrochemical redox reactions. (a) Cyclic voltammograms (CVs) for the prepared 45 nm $LiFePO_4$ (LFP) nanoparticles in 0.5 M Li_2SO_4 aqueous electrolyte using Pt wire as the counter electrode and Ag/AgCl as the reference electrode, and 1 mol L^{-1} $LiClO_4$ organic electrolyte (a mixture of ethylene carbonate and dimethyl carbonate) at the scan rate of 20 mV s^{-1}. Note that separations between cathodic and anodic peaks in aqueous (~0.1 V) are much smaller than that in nonaqueous (~0.5 V) electrolyte. Electrochemical kinetics numerical simulations are adopted to fit the redox peaks in the CVs (green lines, section S1 in Supporting Information), where electrochemical kinetics process model was adopted while taking into account the anodic and cathodic peak shifts upon the change of scanning rate. (b) Change of mass during the CV scan measured by EQCM in charge process and discharge process (inset), respectively. M_A and M_O denote the change of mass induced by every molar electrons in the aqueous electrolyte and the organic electrolyte, respectively.

The voltage profiles as functions of capacity (the degree of intercalations) at varying CDRs are described in Figure 1c and d in 0.5 M Li_2SO_4 aqueous electrolyte and in 1 M $LiClO_4$ in ethylene carbonate (EC) and dimethyl carbonate (DMC), respectively. Note that ultrahigh charging and discharging curves in the aqueous and organic electrolytes are symmetric (Figure 1c and d), and there are voltage platforms (close to 3.5 V vs Li^+/Li) in the charge and discharge curves (Figure 1c and d), which is a typical behavior for $LiFePO_4$ and can be clearly seen up to 600 C in aqueous electrolyte and up to 120 C (1 C = 170 mAh g^{-1}) in organic electrolyte. The drop of the voltage of the platform with the increasing charge and discharge rate is due to the increasing polarization. We can see that at ultrahigh charging rates of 600 C, a capacity of 72.0 mAh g^{-1} (42% of the theoretical capacity) was retained in the aqueous electrolyte (Figure 1c and Supporting Information Figure S2). Compared with the $LiFePO_4$ nanoparticles prepared similarly but evaluated in organic electrolytes, where the accessible capacity sharply decreases to 20 mAh g^{-1} at 200 C (Figure 1d), the rate capability in aqueous electrolyte is apparently much superior. Here, we also measured the capacity of the carbon (acetylene black) under the same experimental conditions and at different current densities. As shown in Figure S3 in Supporting Information, the acetylene black exhibits very low capacity both in aqueous and organic electrolytes at high current rates, so the capacity of carbon could be ignored in the working electrode (mixing of $LiFePO_4$/C, acetylene black and PTFE). Furthermore, in order to get the exact capacity of the intrinsic $LiFePO_4$ particles at charging rate of 600 C, we first charged the battery at 600 C, the initial state of the cathode is $LiFePO_4$) and then measured the capacity under low discharging rate (e.g., 3 C discharge rate) (Figure S4a in Supporting Information). Similarly, to get the capacity at discharging rate of 600 C, we first discharged the battery at 600 C (the initial state of the cathode is $FePO_4$) and then measured the capacity under low charge rate (e.g., 3 C charge rate) (Figure S4b in Supporting Information). We can see that there are clear voltage platforms in the 3 C discharging and 3 C charging curves, and the capacities at 3 C discharge rate and 3 C charging rate should reflect the exact capacity of delithiation from the intrinsic $LiFePO_4$ particles at charging rate of 600 C and lithiation from the $FePO_4$ particles at discharging rate of 600 C, respectively.

We also found that this ultrahigh rate capability in aqueous electrolyte comes with excellent cycling stability (Figure S6 in Supporting Information), that is, the loss of capacity is only 5% after 400 cycles at 10 C, or <15% after 1000 cycles for 45 nm $LiFePO_4$ crystal. Additional nanostructure and hierarchy were also introduced to $LiFePO_4$ when a hybrid nanohollow composite with the mean pore sizes of 200 nm was assembled with multiwall carbon nanotubes (MWCNTs) (Figure S7 in Supporting Information), which affords similar CDR and cycling stability in aqueous electrolyte; that is, capacities retained at the rates of 120, 300, and 600 C are 97.6, 84.0, and 62.6 mAh g^{-1}, or 60%, 58%, 50%, and 38% of the theoretical capacity, respectively. Compared with the previously reported CDR in aqueous electrolyte,[16] the higher rates achieved here are most likely due to better optimized carbon coating and higher electronic conductivity. Calculation shows that, at the same electronic conductivity and electrode surface-to-volume ratio, CDR in aqueous media could be higher than in nonaqueous electrolytes nearly by 5 times; the underlying mechanism governing this tremendous difference, however, has not been accounted for.

One intuitive explanation for the higher CDR in aqueous electrolyte would resort to the higher Li^+-diffusion rate (or conductivity) therein.[24] Upon closer examination, however, one would readily rule out this factor because the ionic conductivity in 0.5 M Li_2SO_4 aqueous electrolyte (1.67 mS cm^{-1}) is only higher than that of nonaqueous electrolyte (1.44 mS cm^{-1} for 1 M $LiClO_4$ in EC/DMC) by a fraction (Table S4 in Supporting Information). Moreover, the high CDR in aqueous electrolyte is insensitive to the concentration of Li^+ in aqueous electrolyte (Table S3 in Supporting Information). These evidence suggest that the Li^+-diffusion in bulk electrolyte should not be the rate-determining step that exercises kinetic control over CDR. This inference is further supported by the numerical analysis on cyclic voltammogram (CV) as shown in Figure 2a and in Figure

DOI: 10.1021/acs.nanolett.5b02379
Nano Lett. 2015, 15, 6102−6109

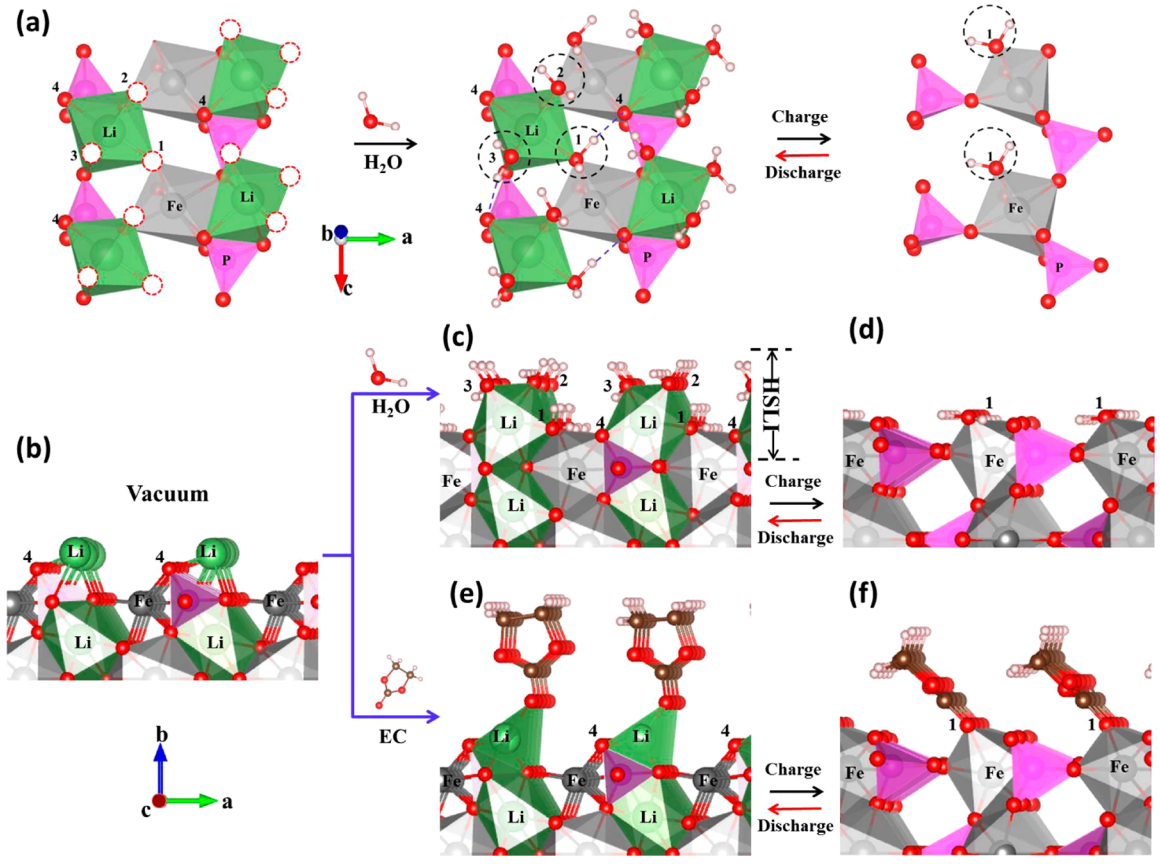

Figure 3. Ab initio calculated H_2O/EC absorption at $LiFePO_4$ and $FePO_4$ surfaces. (a) Top view of $LiFePO_4$/vacuum, $LiFePO_4/H_2O$, and $FePO_4/H_2O$ at (010) direction. The four LiO_6 octahedrons correspond to four Li diffusion channels. The dashed red cycles denote the O vacancies at the surface. (b) to (d) Side view of $LiFePO_4$/vacuum, $LiFePO_4/H_2O$, and $FePO_4/H_2O$ at (010) direction, respectively. "HSLI" denotes the hydrated solid−liquid interface. (e) and (f) Side view of $LiFePO_4$/EC and $FePO_4$/EC at (010) direction, respectively.

S8a in Supporting Information, where electrochemical kinetics process model (see section S3 in Supporting Information for details) was adopted while taking into account the anodic and cathodic peak shifts upon the change of scanning rate. As visually hinted by the separations between cathodic and anodic peaks, which is much smaller in aqueous (~0.1 V) with minimum overpotential than that in nonaqueous (~0.5 V) electrolyte, the overall (surface plus bulk) Li^+-diffusion constant within $LiFePO_4$ nanoparticles when evaluated in aqueous electrolyte is higher by an order of magnitude than the corresponding values if evaluated in nonaqueous electrolytes, that is, 5.0×10^{-11} cm^2/s versus 5.0×10^{-12} cm^2/s. Apparently, this gap should be the defining factor for the much higher CDR realized in aqueous-based LIB. Additional evidence comes from the electrochemical impedance spectra, where the interfacial resistance observed for the same nanosized $LiFePO_4$ is much smaller in aqueous electrolyte (Figures S8b and S9b in Supporting Information). Because Li^+-diffusions inside the nanoparticles of the same source should be independent from the electrolytes used, either aqueous or nonaqueous, the difference has to arise from the corresponding solid/liquid interfaces. This would explain why the modeled overall diffusion constant 5.0×10^{-11} cm^2/s is much lower than the theoretical bulk Li^+-diffusion constant ($1.0 \times 10^{-8} \sim 1.0 \times 10^{-10}$ cm^2/s) within $LiFePO_4$.[26]

For the aqueous scenario, the Coulombic efficiency is 100% even at the first cycle, indicating a simple redox process without Li loss. This perhaps should be attributed to the moderate redox potential (3.5 V) of $LiFePO_4$, which is not high enough to require the formation of an interphase,[2] differing from mainstream metal oxide cathodes such as $LiCoO_2$, $LiNiO_2$, $LiNi_xCo_yMn_zO_2$, and $LiMn_2O_4$ that operate beyond 4.0 V.[27−29] This simple $LiFePO_4$/electrolyte *interface* in absence of *interphase* makes it ideal for ab initio theoretical investigations under the density functional theory (DFT). It should be emphasized here that the carbon coating does not block the electrolyte from directly accessing the $LiFePO_4$ surfaces.[29,30] In our model, the (010) surface of $LiFePO_4$ (Figure 3a and b) is selected as the contact surface with electrolyte, which is normal to the bulk Li diffusion channel.[31] In such a 2-D classical interface, the inner-Helmholtz structure of $LiFePO_4$ surfaces constitutes the key conduction passage for Li^+. The H_2O adsorption at different atomic sites on $LiFePO_4$ (010) surface, hence, was calculated with varying numbers of H_2O molecules (section S4 in Supporting Information), and the most stable structure is identified when three H_2O molecules adsorb at three different sites as illustrated in Figure 3a and c (the 1, 2, 3 sites). These sites are the exact locations of the O vacancy at the corners of FeO_6 and LiO_6 octahedrons in a stoichiometric (010) $LiFePO_4$ surface. The O atoms from the adsorbed H_2O molecules fill in such vacancies and complete the originally truncated octahedral coordination symmetry. In particular, at the concave site 1 (Figure 3a and c), the O from H_2O completes both a FeO_6 and a LiO_6 octahedron, with a H_2O-to-surface binding energy being 1.37 eV. The H atom from the same H_2O molecule also forms a strong hydrogen bond with

DOI: 10.1021/acs.nanolett.5b02379
Nano Lett. 2015, 15, 6102−6109

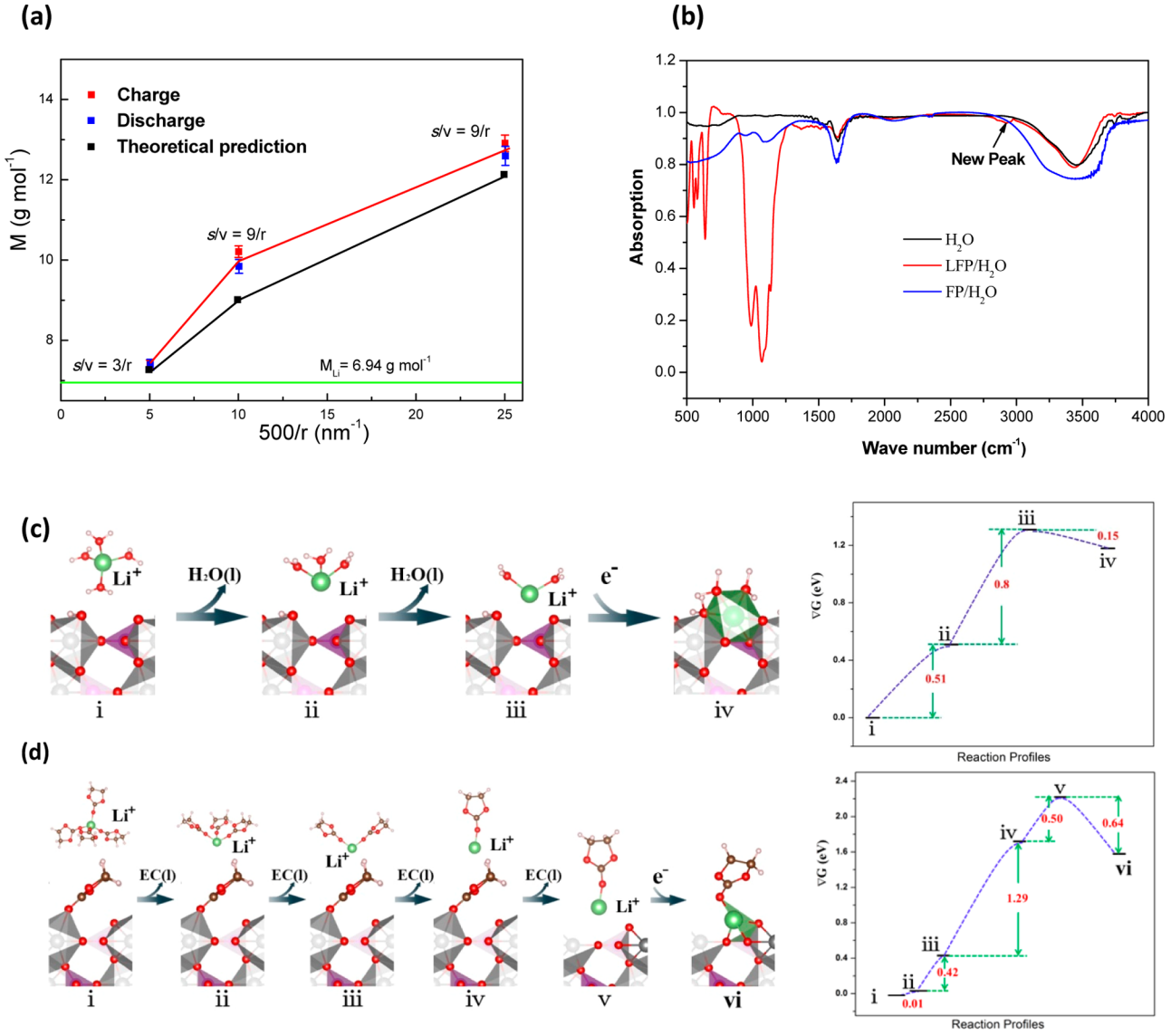

Figure 4. Experimental evidence for the optimized hydrated interface and the reaction profiles for Li-ions transport across the $FePO_4$/water interface and $FePO_4$/EC interface. (a) Total change of mass (M) induced by every molar electrons during the CV scan for charge (red line and dots) and discharge (blue dots) process versus the average $LiFePO_4$ particle size ($l = 2r$) in 0.5 M Li_2SO_4 aqueous electrolyte. (b) Fourier transform infrared (FTIR) spectra for water, water with LFP, and water with FPO. (c) and (d) Reaction profiles for Li-ions transport across the $FePO_4$/water interface (c) and $FePO_4$/EC interface (d) in the discharge process and their energies at each step (right-hand panels). Li, green; Fe, gray; P, purple; O, red; C, brown; H, white.

the neighboring O atom at site 4, pulling this $O_{(site\ 4)}$ atom toward it by about 0.2 Å (Figure 3a). Note that, beside these three H_2O molecules, no other water molecule has direct access to the $LiFePO_4$ interface. Such unique arrangement of water molecules at those $LiFePO_4$ (010) sites actually creates a "Janus" interface in the key Li^+-passage that simulates the structures of both solid (electrode) and liquid (electrolyte) phases (Figure 3c). It has been well-established in surface sciences that interfaces of such properties are effective in promoting fast mass transfer.[32,33] Water adsorption was also calculated at the fully delithiated $FePO_4$ surfaces. In this case, except the site 1 for the FeO_6 octahedron, the O vacancy sites of LiO_6 octahedron no longer exist. As a result, only one H_2O molecule can be accommodated at the surface at site 1 (Figure 3a and d) with a binding energy of 0.97 eV. On the basis of the above first-principles models, a simple schematic illustration of solid/liquid interfaces of $LiFePO_4$/water, $FePO_4$/water, $LiFePO_4$/EC, and $FePO_4$/EC is shown in Figure S16 in Supporting Information.

The transition from "tri-H_2O molecule bound to $LiFePO_4$ surface" to "mono-H_2O molecule bound to $FePO_4$ surface" is further verified with an accurate in situ mass measurement, that is, electrochemical quartz crystal microbalance (EQCM). During the charging/discharging process, EQCM in the aqueous electrolyte shows that every molar electron (as determined from the electric current passed) is accompanied by a decrease or increase of 12.6/12.9 g mol^{-1} mass change (Figure S19 in Supporting Information and red lines in Figure 2b), which is 5.66/5.96 g mol^{-1} in excess of the deintercalation/intercalation of one Li^+ (6.94 g mol^{-1}). This change in mass is stable and reversible during the electrochemical charging and discharging. In contrast, mass change per molar electron as registered by EQCM becomes 6.6–6.7 g mol^{-1} in nonaqueous electrolyte, consistent with the mass

DOI: 10.1021/acs.nanolett.5b02379
Nano Lett. 2015, 15, 6102–6109

change of one Li^+ (blue lines in Figure 2b). In a multi-nanoparticle electrode, it has been well established that one nanoparticle will be fully charged (or discharged) before other nanoparticles start to participate the reaction. Thus, this mass change during the charging/discharging process should correspond to mass change between pure $LiFePO_4$ and pure $FePO_4$ nanoparticles, that is, the change from tri-H_2O molecule adsorptions to mono-H_2O adsorption. Using such a model, the excess mass can be calculated while taking into account the particle size and the surface areas (section S5 in Supporting Information). The calculated excess mass agrees well with the excess mass as measured by EQCM for different nanoparticle sizes as shown in Figure 4a. This is by far the most compelling evidence for the reversible adsorption/desorption of water molecules during the charging/discharging process because there is no other plausible explanation for the measured excess mass change. Fourier transform infrared spectroscopy (FTIR) was also used to study the microstructure of surface H_2O adsorption (section S6 in Supporting Information). The phonon modes related to H−O bond bending and stretching is of particular interest, because this mode at about 3500 cm^{-1} does not overlap with other phonon modes. For the $LiFePO_4$/H_2O system (red line in Figure 4b), an additional small peak around 2800 cm^{-1} (compared to the simple summation of $LiFePO_4$ and H_2O FTIRs) was observed, which was down shifted from the original H−O stretching mode main peak at 3500 cm^{-1}. DFT calculations of the phonon modes using the atomic structure of $LiFePO_4{\cdot}3H_2O$ (Table S6 in Supporting Information) also show a soft $O_{(site\ 1)}$−H stretching mode of 2500 cm^{-1} (shifted from the main peak around 3400 cm^{-1}), which arises due to the strong hydrogen bond along the $O_{(site\ 1)}$−H−$O_{(site\ 4)}$ in Figure 3a, while weakening the O−H bond strength. Due to possible complication of other H_2O molecules and the deficiency of using DFT to accurately describe the hydrogen bond, a more quantitative comparison is not possible at the moment. However, the FTIR does qualitatively support our picture of water-binding. Note that in the case of $FePO_4{\cdot}H_2O$, both the FTIR and DFT calculation do not show any significant sharp features (Figure 4b and Table S5 in Supporting Information).

The above water absorption picture provides a possible scenario for Li ion diffusion at the solid/liquid interface (section S7 in Supporting Information). At zero or partial intercalation (Li_xFePO_4 where $0 \le x \le 1.0$), the Li^+ will be accommodated inside the nanocrystal to form a solid solution as proposed by Malik et al.[12] As a result, the surface can be considered as a pure $FePO_4$ phase and only one water molecule is required to compensate the truncated octahedral symmetry (Figure 3a). Only once full intercalation along any Li channel to generate Li_xFePO_4 phase in this nanoparticle, three H_2O would be required at the surface of the Li channel. On the other hand, it is already known that each Li^+ in aqueous electrolyte is always coordinated by four water molecules in its primary solvation sheath, forming a complex cation $Li^+(H_2O)_4$.[34−36] In order for a Li^+ to intercalate into the nanoparticle, two but only two water molecules need to be stripped away from this complex (i to ii, and to iii in Figure 4c). Following this initially partial desolvation, the resultant $Li^+(H_2O)_2$ can approach the $LiFePO_4$ surface with almost no additional barrier and docks at the site (iii to iv in Figure 4c) to form a structure similar to the scenario of $3H_2O$ on top of $LiFePO_4$ of Figure 3a. After this Li^+ diffused into the $LiFePO_4$ bulk along the Li channel, these two H_2O will desorb from the surface. The DFT calculated energies of these intermediate stages are shown in Figure 4c, and all the major energy barriers were proven to originate from Li^+-desolvation process at the interface instead of within either electrolyte or electrode bulk. Note that, due to the small size of H_2O molecule, the $Li^+(H_2O)_4$ can intimately approach those concaves with truncated symmetries before desolvation occurs, making it possible for the surface electric field to facilitate the desolvation process, and hence further reduce the energy barriers of the discharging process from the ones shown in Figure 4c.

Following the same procedure, the possible interaction between nonaqueous solvent EC molecule and $LiFePO_4$ (010) surface is also evaluated. Previously, it has been found that EC is the preferred solvent member in the primary solvation sheath of Li^+ despite the dominant DMC presence.[37] It was found that for both $LiFePO_4$ and $FePO_4$, only one EC molecule can be adsorbed due to steric hindrance (Figure 3e and f), and three EC molecules need to be desolvated from the complex cation $Li^+(EC)_4$[38,39] before it can approach the concaves at (010) surface in order for the intercalation of one Li^+ to happen. This not-so-intimate interaction fails to compensate the truncated solid symmetry at those (010) channels, and Li^+ must overcome a higher energy barriers to cross such interfaces, as shown in Figure 4d and consistent with earlier electrochemical experiments, where the height of the barrier was estimated to be as high as 50 kJ/mol.[40] Likewise, the desolvation process in nonaqueous electrolytes has to happen far away from the surface due to the large EC molecule size, which makes its desolvation less likely to be assisted by the surface electric field. Combination of all these factors led to the much higher barrier for Li^+ to cross such a solid/liquid interface, resulting in much lower CDR. We calculated the potential barriers for the charging process using the same approach, and the results are shown in Figure S24 in Supporting Information. Similarly, we saw a lower barrier for the aqueous electrolyte than the nonaqueous electrolyte thanks to the optimized interface created by the water adsorption.

Conclusions. In summary, Janus solid−liquid interface was created by the unique arrangement of water molecules at the specific (010) sites of $LiFePO_4$, whose partial-solid and partial-liquid structure compensates the truncated surface symmetry of the former, and serves as a transition state during the Li^+-transport across the electrolyte/electrode interface. This coordination of Li^+ by O_s and O_L from solid electrode and liquid electrolyte respectively relieves the energy barriers associated with the Li^+-desolvation process, leading to minimum overpotential and a least-resisting interface that are responsible for the ultrahigh CDR observed. Energy storage devices constructed upon such nanosized $LiFePO_4$ in aqueous electrolytes are expected to demonstrate both unprecedented rate capability and maximum round trip efficiency for energy conversion during the operation. Of more fundamental and broader significance, the above picture of $LiFePO_4$ (010) surface in water actually represents what an ideal interface shouldbe it adopts a transition structure (symmetry) that closely imitates the interior bulk of both phases so that a mobile species would experience the minimum discontinuities in properties while transporting across such interfaces. We believe that this should be the principle that guides the rational design of a perfect interface of ultrafast transport properties.

Methods Section. *Experimental Section.* The $LiFePO_4$ particles with mean size of 45 nm (calculated from Scherrer equation) were synthesized by reflux route in ethylene glycol

DOI: 10.1021/acs.nanolett.5b02379
Nano Lett. 2015, 15, 6102−6109

solution under atmospheric pressure. In a typical route, $FeSO_4 \cdot 7H_2O$, H_3PO_4, and $LiOH \cdot H_2O$ were used as starting materials in a molar ratio of 1:1.5:2.7 and ethylene glycol (EG) was applied as solvent. H_3PO_4 was slowly introduced to the LiOH solution under stirring, and then $FeSO_4$ solution was added into the mixture. After homogenization, the reaction mixture was heated at reflux condition for 10 h under Ar atmosphere. The resulting suspension was washed several times with water and ethanol. To achieve carbon coating, $LiFePO_4$ nanoparticles were mixed with 20 wt % of glucose and then carbonized at 650 °C for 6 h in Ar atmosphere. For the synthesis of $LiFePO_4$ nanoparticles with mean size of 101 nm (calculated from Scherrer equation), the feeding sequence was changed. In this case, H_3PO_4 was slowly introduced to the $FeSO_4$ solution under stirring. Then LiOH solution was added into the mixture. Other steps are the same as the synthetic process for 45 nm $LiFePO_4$ particles.

The working electrode was prepared by pressing a mushy mixture of the prepared composite, acetylene black and poly(tetrafluoroethylene) (PTFE) (weight ratio: 30:50:20) dispersed in isopropanol onto steel grid. The thickness of the electrode was about 50 μm, and its area was about 0.3 cm^2. The active materials mass loading is 0.8 mg. The electrode area was about 0.3 cm^2 and its weight was about 0.8 mg. Aqueous Li_2SO_4 electrolyte (0.5 M) was used as the electrolyte. Galvanostatic charge−discharge tests (Maccor, MC-16 Battery Test System) of the $LiFePO_4$/C composites electrodes were performed using a three-electrode cell, where the active carbon and saturated calomel electrode (SCE) were used as counter and reference electrodes, respectively. Pt wire and Ag/AgCl were used as the counter and reference electrodes in cyclic voltammetry (CV) and electrochemical impedance (CHI 660E, Shanghai Chenhua). The electrochemical impedance spectra were recorded from 10^4 to 0.1 Hz and the amplitude of the used perturbation was 10 mV. For the EQCM test on an electrochemical workstation (CHI 440B, Shanghai Chenhua), the $LiFePO_4$ particles were deposited on the gold disk which was coated on the crystal plate. Ionic conductivities of the electrolyte solutions were measured at room temperature using a Model DDS-307 conductometer (Shanghai REX Instrument Factory, China).

Theoretical. All calculations are performed using the plane-wave projector-augmented wave method[41] with an energy cutoff of 520 eV, as implemented in the Vienna ab initio simulation package (VASP).[42−46] The Perdew−Burke−Ernzerhof (PBE)[47] form of generalized gradient approximation (GGA) is chosen as the exchange-correlation potential. The PBE+U approach[48] is employed to take account of the strong on-site Coulomb interaction (U) presented in the localized 3d electrons of Fe, with the U values set to 4.7 eV in $LiFePO_4$ and 5.9 eV in $FePO_4$. To obtain reliable optimized structures and the total energy, all the atomic positions and cell parameters are fully relaxed using a conjugate gradient algorithm, until the force on each atom is smaller than 0.02 eV/Å and energies are converged to within 5×10^{-6} eV per atom. A $8 \times 4 \times 1$ k-point grid within the Monkhorst−Pack scheme[49] is used to sample the Brillouin zone of the $LiFePO_4$ (010) surface unit cell, and a $1 \times 1 \times 1$ k-point grid is used for calculations of separate molecules. We finally employed a climbing-image nudged elastic band (cNEB) method[50] to calculate the energy barriers for Li atoms diffusion in the bulk $LiFePO_4$ ($FePO_4$) and from the subsurface to the surface. A DFT-D_2 semiempirical dispersion-correction approach[51] to correct the van der Waals (vdW) interactions and a dipole correction method are also tested in our calculations, and we find there is little influence to the final optimized structures. A ferromagnetic high-spin Fe state is assumed, and the energetic effects of the magnetic ordering are small. In order to study the interfacial properties between $LiFePO_4$/$FePO_4$ surfaces and electrolytes, we build a 1×2 ($a \times c$) bilayer $LiFePO_4$/$FePO_4$ (010) slab to simulate the $LiFePO_4$/$FePO_4$ (010) surface. A vacuum buffer space of at least 12 Å is set for slabs with adsorbed molecules. Lattice parameters of the supercell (including slab and vacuum) are fixed, and the inner part of the slab is frozen at the bulk positions and only the atoms near the surface are allowed to relax. The electron counting rule[52,53] and the surface reconstruction are also considered. The vibrational modes are calculated based on the numerical calculations of the second derivatives of the potential energy within the harmonic approximation.

Additional details on materials and methods are included in the Supporting Information.

■ ASSOCIATED CONTENT

Supporting Information

The Supporting Information is available free of charge on the ACS Publications website at DOI: 10.1021/acs.nanolett.5b02379.

Additional materials and methods; additional materials characterization and electrochemical performances; electrochemical kinetics analysis; ab initio calculation results; the mass change for $LiFePO_4$ during charging and discharging process versus the average $LiFePO_4$ particle size; Fourier transform infrared (FTIR) spectra observation and vibrational modes calculations for the interface structure; detailed discussions for the discharge and charge process. (PDF)

■ AUTHOR INFORMATION

Corresponding Authors

*E-mail: wuyp@fudan.edu.cn.

*E-mail: panfeng@pkusz.edu.cn.

Author Contributions

These authors contributed equally to this work (J.Z., Y.H., Y.D).

Notes

The authors declare no competing financial interest.

■ ACKNOWLEDGMENTS

The research was financially supported by National Project for EV Batteries (20121110, OptimumNano, Shenzhen), National Distinguished Young Scientists of China (51425301), STCSM (12JC1401200), Guangdong Innovation Team Project (No. 2013N080), and Shenzhen Science and Technology Research Grant (No. ZDSY20130331145131323 and CXZZ20120829172325895). L.W.W. is supported through the Theory of Material project by the Director, Office of Science (SC), Basic Energy Science (BES)/Materials Science and Engineering Division (MSED) of the U.S. Department of Energy (DOE) under the contract No. DE-AC02-05CH11231. Additionally, we acknowledge the support of ShenZhen National Super Computing Center.

■ REFERENCES

(1) Xu, K. *Chem. Rev.* **2004**, *104*, 4303−4418.

DOI: 10.1021/acs.nanolett.5b02379
Nano Lett. 2015, 15, 6102−6109

(2) Xu, K. *Chem. Rev.* **2014**, *114*, 11503−11618.
(3) Jow, T. R.; Xu, K.; Borodin, O.; Ue, M. *Electrolytes for lithium and lithium-ion batteries*; Springer: New York, 2014; *Vol. 58*.
(4) Dunn, B.; Kamath, H.; Tarascon, J.-M. *Science* **2011**, *334*, 928−935.
(5) Yang, Z. G.; Zhang, J.; Kintner-Meyer, M. C.; Lu, X. C.; Choi, D.; Lemmon, J. P.; Liu, J. *Chem. Rev.* **2011**, *111*, 3577−3613.
(6) Presser, V.; Dennison, C. R.; Campos, J.; Knehr, K. W.; Kumbur, E. C.; Gogotsi, Y. *Adv. Energy Mater.* **2012**, *2*, 895−902.
(7) Halls, J. E.; Hawthornthwaite, A.; Hepworth, R. J.; Roberts, N. A.; Wright, K. J.; Zhou, Y.; Haswell, S. J.; Haywood, S. K.; Kelly, S. M.; Lawrence, N. S.; Wadhawan, J. D. *Energy Environ. Sci.* **2013**, *6*, 1026−1041.
(8) Arico, A. S.; Bruce, P.; Scrosati, B.; Tarascon, J.-M.; van Schalkwijk, W. *Nat. Mater.* **2005**, *4*, 366−377.
(9) Whittingham, M. S. *Chem. Rev.* **2014**, *114*, 11414−11443.
(10) Gaberscek, M.; Kuzma, M.; Jamnik, J. *Phys. Chem. Chem. Phys.* **2007**, *9*, 1815−1820.
(11) Liu, J.; Kunz, M.; Chen, K.; Tamura, N.; Richardson, T. J. *J. Phys. Chem. Lett.* **2010**, *1*, 2120−2123.
(12) Malik, R.; Abdellahi, A.; Ceder, G. *J. Electrochem. Soc.* **2013**, *160*, A3179−A3197.
(13) Ravet, N.; Chouinard, Y.; Magnan, J. F.; Besner, S.; Gauthier, M.; Armand, M. *J. Power Sources* **2001**, *97*−*98*, 503−507.
(14) Gaberscek, M.; Dominko, R.; Jamnik, J. *Electrochem. Commun.* **2007**, *9*, 2778−2783.
(15) Jansen, A. N.; Dees, D. W.; Abraham, D. P.; Amine, K.; Henriksen, G. L. *J. Power Sources* **2007**, *174*, 373−379.
(16) He, P.; Zhang, X.; Wang, Y. G.; Cheng, L.; Xia, Y. Y. *J. Electrochem. Soc.* **2008**, *155*, A144−A150.
(17) Dathar, G. K. P.; Sheppard, D.; Stevenson, K. J.; Henkelman, G. *Chem. Mater.* **2011**, *23*, 4032−4037.
(18) Wang, Q.; Zakeeruddin, S. M.; Exnar, I.; Grätzel, M. *J. Electrochem. Soc.* **2004**, *151*, A1598−A1603.
(19) Abe, T.; Sagane, F.; Ohtsuka, M.; Iriyama, Y.; Ogumi, Z. *J. Electrochem. Soc.* **2005**, *152*, A2151−A2154.
(20) Li, W.; Dahn, J.; Wainwright, D. *Science* **1994**, *264*, 1115−1118.
(21) Luo, J.-Y.; Cui, W.-J.; He, P.; Xia, Y.-Y. *Nat. Chem.* **2010**, *2*, 760−765.
(22) Tang, W.; Liu, L.; Zhu, Y.; Sun, H.; Wu, Y.; Zhu, K. *Energy Environ. Sci.* **2012**, *5*, 6909−6913.
(23) Tang, W.; Hou, Y.; Wang, F.; Liu, L.; Wu, Y.; Zhu, K. *Nano Lett.* **2013**, *13*, 2036−2040.
(24) Tang, W.; Zhu, Y. S.; Hou, Y. Y.; Liu, L.; Wu, Y. P.; Loh, K. P.; Zhang, H. p.; Zhu, K. *Energy Environ. Sci.* **2013**, *6*, 2093−2104.
(25) Wang, X. J.; Hou, Y. Y.; Zhu, Y. S.; Wu, Y. P.; Holze, R. *Sci. Rep.* **2013**, *3*, 1401.
(26) Malik, R.; Burch, D.; Bazant, M.; Ceder, G. *Nano Lett.* **2010**, *10*, 4123−4127.
(27) Edström, K.; Gustafsson, T.; Thomas, J. O. *Electrochim. Acta* **2004**, *50*, 397−403.
(28) Dupré, N.; Martin, J.-F.; Degryse, J.; Fernandez, V.; Soudan, P.; Guyomard, D. *J. Power Sources* **2010**, *195*, 7415−7425.
(29) Akita, Y.; Segawa, M.; Munakata, H.; Kanamura, K. *J. Power Sources* **2013**, *239*, 175−180.
(30) Zaghib, K.; Dontigny, M.; Charest, P.; Labrecque, J. F.; Guerfi, A.; Kopec, M.; Mauger, A.; Gendron, F.; Julien, C. M. *J. Power Sources* **2008**, *185*, 698−710.
(31) Wang, L.; Zhou, F.; Meng, Y. S.; Ceder, G. *Phys. Rev. B* **2007**, *76*, 165435.
(32) de Gennes, P. G. *Angew. Chem., Int. Ed. Engl.* **1992**, *31*, 842−845.
(33) Hu, J.; Zhou, S.; Sun, Y.; Fang, X.; Wu, L. *Chem. Soc. Rev.* **2012**, *41*, 4356−4378.
(34) Rudolph, W.; Brooker, M. H.; Pye, C. C. *J. Phys. Chem.* **1995**, *99*, 3793−3797.
(35) Pye, C. C.; Rudolph, W.; Poirier, R. A. *J. Phys. Chem.* **1996**, *100*, 601−605.
(36) Mähler, J.; Persson, I. *Inorg. Chem.* **2011**, *51*, 425−438.
(37) von Cresce, A.; Xu, K. *Electrochem. Solid-State Lett.* **2011**, *14*, A154−A156.
(38) Yanase, S.; Oi, T. *J. Nucl. Sci. Technol.* **2002**, *39*, 1060−1064.
(39) Bogle, X.; Vazquez, R.; Greenbaum, S.; Cresce, A. v. W.; Xu, K. *J. Phys. Chem. Lett.* **2013**, *4*, 1664−1668.
(40) Xu, K.; von Cresce, A.; Lee, U. *Langmuir* **2010**, *26*, 11538−11543.
(41) Blöchl, P. *Phys. Rev. B: Condens. Matter Mater. Phys.* **1994**, *50*, 17953−17979.
(42) Kresse, G.; Furthmüller, J. *Comput. Mater. Sci.* **1996**, *6*, 15−50.
(43) Kresse, G.; Furthmüller, J. *Phys. Rev. B: Condens. Matter Mater. Phys.* **1996**, *54*, 11169−11186.
(44) Kresse, G.; Hafner, J. *Phys. Rev. B: Condens. Matter Mater. Phys.* **1993**, *47*, 558−561.
(45) Kresse, G.; Hafner, J. *Phys. Rev. B: Condens. Matter Mater. Phys.* **1994**, *49*, 14251−14269.
(46) Kresse, G.; Joubert, D. *Phys. Rev. B: Condens. Matter Mater. Phys.* **1999**, *59*, 1758−1775.
(47) Perdew, J.; Burke, K.; Ernzerhof, M. *Phys. Rev. Lett.* **1996**, *77*, 3865−3868.
(48) Anisimov, V.; Zaanen, J.; Andersen, O. *Phys. Rev. B: Condens. Matter Mater. Phys.* **1991**, *44*, 943−954.
(49) Monkhorst, H.; Pack, J. *Phys. Rev. B* **1976**, *13*, 5188−5192.
(50) Henkelman, G.; Uberuaga, B. P.; Jónsson, H. *J. Chem. Phys.* **2000**, *113*, 9901−9904.
(51) Tkatchenko, A.; Scheffler, M. *Phys. Rev. Lett.* **2009**, *102*, 073005.
(52) Tasker, P. *J. Phys. C: Solid State Phys.* **1979**, *12*, 4977−4984.
(53) Manna, L.; Wang; Cingolani, R.; Alivisatos, A. P. *J. Phys. Chem. B* **2005**, *109*, 6183−6192.

DOI: 10.1021/acs.nanolett.5b02379
Nano Lett. 2015, 15, 6102−6109